Supporting Online Material for

Antibody Recognition of a Highly Conserved Influenza Virus Epitope

Damian C. Ekiert, Gira Bhabha, Marc-André Elsliger, Robert H. E. Friesen, Mandy Jongeneelen, Mark Throsby, Jaap Goudsmit, Ian A. Wilson*

*To whom correspondence should be addressed. E-mail: wilson@scripps.edu

Published 26 February 2009 on *Science* Express
DOI: 10.1126/science.1171491

This PDF file includes:

Supporting Online Material MS #1171491

Antibody recognition of a highly conserved influenza virus epitope: implications for universal prevention and therapy

Damian C. Ekiert,[1] Gira Bhabha,[1] Marc-André Elsliger,[1] Robert H. E. Friesen,[2] Mandy Jongeneelen, [2] Mark Throsby,[2] Jaap Goudsmit,[2] Ian A. Wilson[1,3*]

[1]Department of Molecular Biology, The Scripps Research Institute, 10550 North Torrey Pines Road, La Jolla, CA 92037, USA.

[2] Crucell Holland BV, Archimedesweg 4-6, 2301 CA Leiden, The Netherlands

[3]The Skaggs Institute for Chemical Biology, The Scripps Research Institute, 10550 North Torrey Pines Road, La Jolla, CA 92037, USA.

*To whom correspondence should be addressed. E-mail: wilson@scripps.edu

Supporting Online Material

Materials and Methods

Cloning, Expression and Purification of the Hemagglutinin and CR6261 Fab

Based on H3 numbering, cDNAs corresponding to residues 11-329 (HA1) and 1-176 (HA2) of the ectodomain of the hemagglutinin (HA) from A/Vietnam/1203/2004 (Viet04/H5; Accession No. AY651334 and AY818135) and A/South Carolina/1/1918 (SC1918/H1; Accession No. AF117241) were fused to an N-terminal gp67 signal peptide and to a C-terminal trimerization domain and His-tag by overlap PCR, essentially as previously described (S*1-3*). The trimerization domain and His-tag were separated from the HA ectodomain by a thrombin cleavage site. The whole cassette was inserted into a baculovirus transfer vector, pFastBacHT-A (Invitrogen). HA protein was produced by infecting suspension cultures of Hi5 cells (Invitrogen) with recombinant baculovirus at an MOI of 5-10 and incubated at 28°C shaking at 110 RPM. After 72 hours, the cultures were clarified by two rounds of centrifugation. The supernatants, containing secreted, soluble HA was concentrated and buffer exchanged into 1xPBS, pH 7.4. The Viet04/H5 HA consisted of a mixture of uncleaved HA0 and cleaved HA1/HA2, while SC1918/H1 was essentially entirely uncleaved. After metal affinity chromatography using Ni-NTA resin, the HAs were digested with trypsin (New England Biolabs, 5mU trypsin per mg HA, 16 hours at 17°C) to produce uniformly cleaved (HA1/HA2), and to remove the trimerization domain and His-tag. After stopping the digests with 2mM PMSF, the digested material purified by anion exchange chromatography and gel filtration, as previously described (S*2, 3*).

CR6261 was expressed recombinantly in mammalian cells as a His-tagged, myc-tagged Fab and purified essentially as previously described (S*4*). The V_H and V_L regions of CR6261

were cloned into a vector containing the C_H1 region of IgG1 and a myc- and His-tag. The Fab fragment was expressed by transient transfection of mammalian cells. Expressed Fab was purified from culture supernatant using a HisTrap™ FF Column (GE Healthcare) and desalted (HiTrap™ Desalting Column, GE Healthcare). The concentration of purified Fab was measured by optical absorbance at 280 nm, and the purity and integrity was analyzed by reducing and non-reducing SDS-PAGE.

Isolation of CR6261-HA complexes

To determine the optimal ratio of Fab to HA to saturate all of the CR6261 binding sites, CR6261 at 1mg/mL was titrated into 10ug SC1918/H1 and Viet-H5 HA. The reactions were allowed to incubate for ~30 minutes at room temperature and binding of the CR6261 Fab to HA was assayed by gel-shift using Blue Native PAGE (Invitrogen).

CR6261 Fab, and purified SC1918/H1 and Viet04/H5 HAs in 10mM Tris pH 8.0, 150mM NaCl at ~1mg/mL, and SC1918/H1 or Viet04/H5 HA in the same buffer at 2mg/mL, were mixed at the optimal ratio determined in the titrations described above (usually estimated to be ~3 Fabs per trimer). The mixtures were incubated overnight at 4˚C to allow complex formation. Saturated complexes were then purified from unbound Fab by gel filtration.

Crystallization and Structure Determination of the CR6261-SC1918/H1 Complex

Gel filtration fractions containing the CR6261-SC1918/H1 complex were concentrated to ~10mg/mL in 10mM Tris, pH 8.0 and 50mM NaCl. Initial robotic crystallization trials were set up using the automated Rigaku Crystalmation robotic system at the Joint Center for Structural Genomics (JCSG). Several hits were obtained, with the most promising candidates grown in

~10% PEG 4K-10K between pH 4.5 and 7.0. Optimization of these conditions resulted in diffraction quality crystals. The crystals used for data collection were grown by the sitting drop vapor diffusion method with a reservoir solution (1mL) containing 10.5% PEG 3K, 100mM sodium acetate 5.2, and 50mM NaCl. Drops consisting of 0.5uL protein + 0.5uL precipitant were set up at 21°C, and crystals appeared within 3-7 days. The resulting crystals were cryoprotected by soaking in well solution supplemented with increasing concentrations of glycerol (5% steps, ~60 seconds each), to a final concentration of 25%, then flash cooled and stored in liquid nitrogen until data collection.

The CR6261-SC1918/H1 dataset was collected to 2.19 Å resolution at the Advanced Photon Source (APS) GM/CA CAT 23-ID-B beamline. Despite strong suspicions that the CR6261-SC1918/H1 dataset was I-centered cubic (e.g., high degree of non-crystallographic symmetry (NCS) and $a \approx b \approx c \approx 202$ Å, $\alpha = \beta = \gamma = 90.00°$ in $I2_12_12_1$), we were unable to index and process it in I23 using HKL2000 (S*5*). However, by integrating in P1 in HKL2000, followed by re-indexing and scaling in Xprep (Bruker), a definitive assignment was made for the CR6261-SC1918/H1 dataset as cubic space group $I2_13$. Detailed data collection and refinement statistics are summarized in Table S1.

The CR6261-SC1918/H1 structure was solved by molecular replacement to 2.2 Å resolution using Phaser (S*6*). A pre-fusion, cleaved SC1918/H1 monomer (PDB code 1RUZ) was used as the initial search model and a single copy was found in the asymmetric unit (S*7*). Examination of the maps at this stage revealed clear positive electron density around the membrane distal end of HA. A subsequent search with a panel of human Fab F_V fragments with lambda chains found a single set of variable domains using 1ADQ (S*8*). However, we were unable to find a convincing molecular replacement solution for the Fab constant domains, either

as a pair, or using the C_H1 and C_L domains separately. After initial rounds of rigid body refinement REFMAC5 and refinement with simulated annealing in Phenix, the maps over HA2 and the F_V region (outside the CDRs, which were not yet rebuilt) were remarkably clear, despite the absence of the constant domains and apparent conformational heterogeneity in HA1 (S*9, 10*). Scattered positive density was observed in the region expected to be occupied by the constant domains, with some continuous density in the vicinity of the elbow region. Manual fitting of the 1ADQ constant domains to the density in Coot allowed the building of several discontinuous segments of 5-20 residues in the both the C_H1 and C_L domains (S*11*).

Examination of the maps over HA1 suggested that the receptor binding and vestigial esterase domains were displaced slightly relative to the unliganded SC1918/H1 structure that was used as a search model. However, rigid body refinement in REFMAC5 (including all of HA1 and various combinations of the receptor binding domain, the vestigial esterase domain, and the membrane proximal regions), refinement with simulated annealing in Phenix, and manual rebuilding failed to yield a substantially better fit to the observed electron density. Simulated annealing omit maps (Phenix), as well as maps generated from the molecular replacement using only HA2 and the Fab, revealed essentially the same result: a loss of features and definition in HA1 when moving from the membrane proximal to membrane distal end of the molecule. Thus, we concluded that the membrane distal end of HA1 is flexible and, hence, partially disordered in our crystals, presumably due to the acidic pH.

Restrained TLS refinement of the structure (using 4-6 TLS groups per chain, determined using TLSMD) was completed in REFMAC5 with model building in Coot (S*12, 13*). Additional positive electron density was observed near all of the 6 potential N-linked glycosylation sites, although the partial disorder of HA1 hampered efforts to build into most of these sites.

However, a total of six sugar residues were built into the density at three positions. Several strong features in the electron density maps remained (still apparent when the F_O-F_C maps were contoured to 5-10σ), ranging in size from roughly 4-20 atoms. Many of these 'unknown' ligands were bound in water-filled cavities around the fusion peptide and along the trimer interface. Some were modeled as glycerol (the cryoprotectant) or ethylene glycol (perhaps a by-product of old or inhomogeneous PEG preparations). A few larger, unknown ligands refined well using ethoxyethanol and tryptophan as models. As we are unable to correlate these latter ligands with any buffer component used at any stage of the purification, crystallization, or cryoprotection process, we have included them in the final coordinates as UNLs. In the late stages of refinement, 293 waters were built into the remaining positive density based upon the following criteria: 1) positive density observed greater than 3σ ; 2) presence of a polar contact within ~3.2 Å ; 3) no negative density on the water after refinement in REFMAC5 ; and 4) no unbuilt glycans or Fab constant regions expected to occupy those remaining features. Thus, somewhat fewer waters have been built into the final model than may have been expected for 2.2 Å resolution, but the number is quite reasonable given the extent of disordered regions as discussed above. Final refinement statistics can be found in Table S1.

Crystallization and Structure Determination of the CR6261-Viet04/H5 Complex

The methods used to determine the CR6261-Viet04/H5 complex structure were very similar to those described above. Briefly, the CR6261-Viet04/H5 complex at ~10mg/mL in 10mM Tris, pH 8.0 and 50mM NaCl was subjected to robotic crystallization trials using the Rigaku Crystalmation System at the JCSG. The hits obtained were very similar to those observed for the CR6261-SC1918/H1 complex. The crystals used for data collection were

grown by the sitting drop vapor diffusion method with a reservoir solution (1mL) containing 12% PEG 6K with 100mM sodium acetate 6.0. 0.5uL + 0.5uL drops were set up at 21°C, and crystals appeared within 3-7 days. The resulting crystals were cryoprotected by soaking in well solution supplemented with increasing concentrations of glycerol (5% steps, ~60 seconds each), to a final concentration of 25%, then flash cooled and stored in liquid nitrogen until data collection.

The CR6261-Viet04/H5 dataset was collected to 2.7 Å resolution at APS GM/CA CAT 23-ID-B beamline. The data were indexed in $P2_13$ and scaled and integrated using Denzo and Scalepack through the HKL2000 package. Detailed data collection and refinement statistics are summarized in Table S1.

The CR6261-Viet04/H5 structure was solved by molecular replacement using Phaser. For the CR6261-Viet04/H5 dataset, three search models were used: the previously determined structure of Viet04/H5 (PDB code 2FK0), the F_V fragment of the CR6261 Fab from the complex structure with SC1918/H1, and the constant domains from 1ADQ. A total of two HA protomers and two Fabs were found in the asymmetric unit. After rigid body refinement REFMAC5 and refinement with simulated annealing in Phenix, examination of the maps revealed that both the HA1 and Fab constant domains were well-ordered in the CR6261-Viet04/H5 complex crystals, with the Fab interacting with the same epitope observed in the CR6261-SC1918/H1 structure. Region B of HA2 (see Fig. 4E) and a strand in the receptor binding domain were found to adopt conformations that were different from the search model, but similar to other H5 structures (S*14*).

Restrained TLS refinement of the structure was completed in REFMAC5 with model building in Coot, essentially as described above. NCS restraints in REFMAC5 and NCS-

averaging using dm were applied during the initial stages of refinement, but released later on to facilitate refinement of the partially divergent N- and C-termini (S*15*). Additional positive electron density was observed near 6 of the 7 non-overlapping potential glycosylation sites in each protomer (12 of the 14 glycosylation sites in the asymmetric unit), with the seventh possessing an Asn-Pro-Thr motif and, therefore, not glycosylated. A total of 11 GlcNAc and mannose residues were built in at 9 of the 14 possible sites (4-5 per protomer). One small ligand was modeled as glycerol (the cryoprotectant) and two as ethylene glycol (perhaps a by-product of old or inhomogeneous PEG preparations). In the late stages of refinement, 164 waters were built into the remaining positive density based upon the following criteria: 1) positive density observed greater than 3σ, 2) presence of a polar contact within ~3.2 Å, 3) no negative density on the water after refinement in REFMAC5, and 4) no unaccounted for glycans or protein side chains expected to occupy that area. Final refinement statistics are summarized in Table S1.

Structural analyses

Hydrogen bonds and van der Waals' contacts between CR6261 and the HAs were calculated using HBPLUS (S*16*) and CONTACSYM (S*17*), respectively. Surface area buried upon Fab binding was calculated with MS (S*18*). The change in the orientation of the CR6261 constant domains between the SC1918/H1 and Viet04/H5 co-crystal structures was analyzed using DynDom (S*19*). MacPyMol (DeLano Scientific) was used to render structure figures and for general manipulations. The final coordinates were validated using the JCSG quality control server (v2.3), which includes Molprobity (S*20*).

Protease susceptibility assays

Each reaction contained 10 μg HA or CR6261-HA complex and 1% dodecyl-maltoside (to prevent aggregation of the post-fusion HA). Reactions were set up at room temperature and the pH was lowered in all samples except controls. Sodium acetate was used for pH ranges 4.9 to 6.1, and PIPES buffer was used for pH ranges 6.3 to 6.9. Reactions were thoroughly mixed, centrifuged at 14,000 RPM for 30 seconds and allowed to incubate at 37 °C for one hour. After incubation, reactions were equilibrated to room temperature and the pH was neutralized by addition of 200 mM Tris, pH 8.5. The actual pH reached during the low pH-treatment (as reported in the figures in the main text) was determined in parallel using larger buffer volumes, but no protein. Trypsin was added to all samples except controls, at a final ratio of 1:50 by mass for the CR6261-Viet04/H5 complex, and 1:25 for the CR6261-SC1918/H1 complex. SC1918/H1 samples were digested overnight (18 hours) at 37 °C and Viet04/H5 samples were digested overnight at 17 °C. Reactions were quenched by addition of non-reducing SDS buffer and were boiled for ~2 min. Samples were analyzed by SDS-PAGE.

To determine the pH required to convert 50% of the HA to the post-fusion form, pH titrations using the assay describing above to monitor conversion. Samples were exposed to a range of pH conditions (pH 4.9, 5.1, 5.3, 5.5, 5.7, 5.9, 6.1, 6.3, 6.5, 6.7 and 6.9) then neutralized and processed as described above. The resulting SDS-PAGE gels were quantified using ImageJ (S*21*) and analyzed using Prism (GraphPad).

Sequence analyses

The NCBI FLU database was queried to return all full-length, non-redundant, non-lab strain influenza A isolates. The search included isolates from all species, all subtypes, and included clones from 1918 through the end of 2008. On the date of access (Jan. 14, 2009), the

database returned a total of 5261 sequences, including 854 H1 (16.2%), 125 H2 (2.4%), 1582 H3 (30.1%), 144 H4 (2.7%), 1384 H5 (26.3%), 261 H6 (5.0%), 359 H7 (6.8%), 17 H8 (0.3%), 334 H9 (6.3%), 59 H10 (1.1%), 71 H11 (1.3%), 25 H12 (0.5%), 26 H13 (0.5%), 2 H14 (0.04%), 5 H15 (0.1%), and 13 H16 (0.25%). The dataset used in the analysis is available upon request. The sequences were aligned using ClustalW+ from the Wisconsin Package/GCG suite (Accelrys). Extraction and manipulation of the data was carried out with custom shell scripts.

In order to account for the difference in the number of sequences available for each subtype (e.g., 2 for H14 but 1582 for H3), the relative frequency of each amino acid was calculated such that frequencies for all amino acids summed to unity at each position. These frequencies were then used for comparisons across subtypes.

Fig. S1. **Crystal structures of CRF6261-bound SC1918-H1 and Viet04-H5 HAs are very similar to unliganded HA structures of the same subtype.** A) Superposition of CRF6261-bound SC1918/H1 (red), unliganded SC1918/H1 (yellow, RMSD 0.69 Å, PDB code 1RUZ), and unliganded A/Puerto Rico/8/1934(H1N1) (blue, RMSD 0.69 Å, PDB code 1RU7). B) Superposition of CRF6261-bound Viet04 (red), unliganded A/Vietnam/1194/2004(H5N1) (blue, RMSD 0.44 Å, PDB code 2IBX).

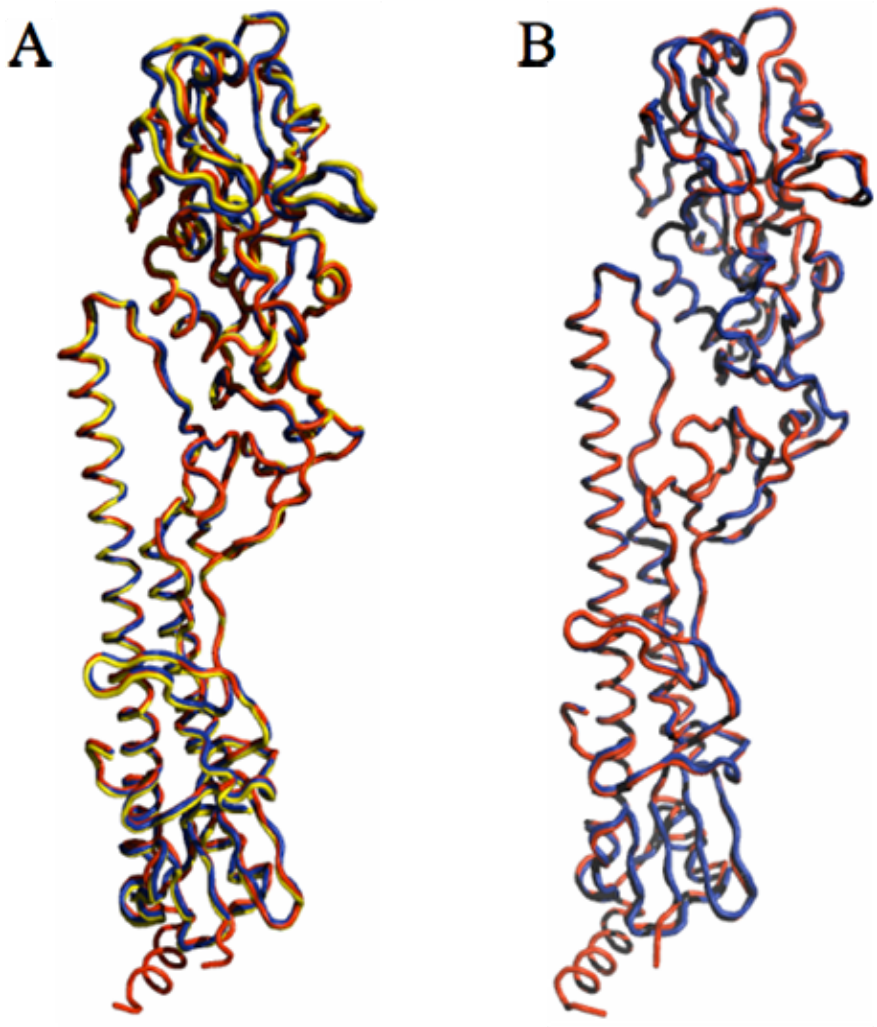

Fig. S2. **The fusion peptide at the N- terminus of HA2 is well ordered and adopts the same location and conformation in unliganded and CR6261- bound SC1918/H1 structures.** A) Superposition of unliganded (blue) and CR6261-SC1918/H1 (red) complex structures. B) Electron density for the fusion peptide in the CR6261-SC1918/H1 complex structure. Map contoured at 2σ.

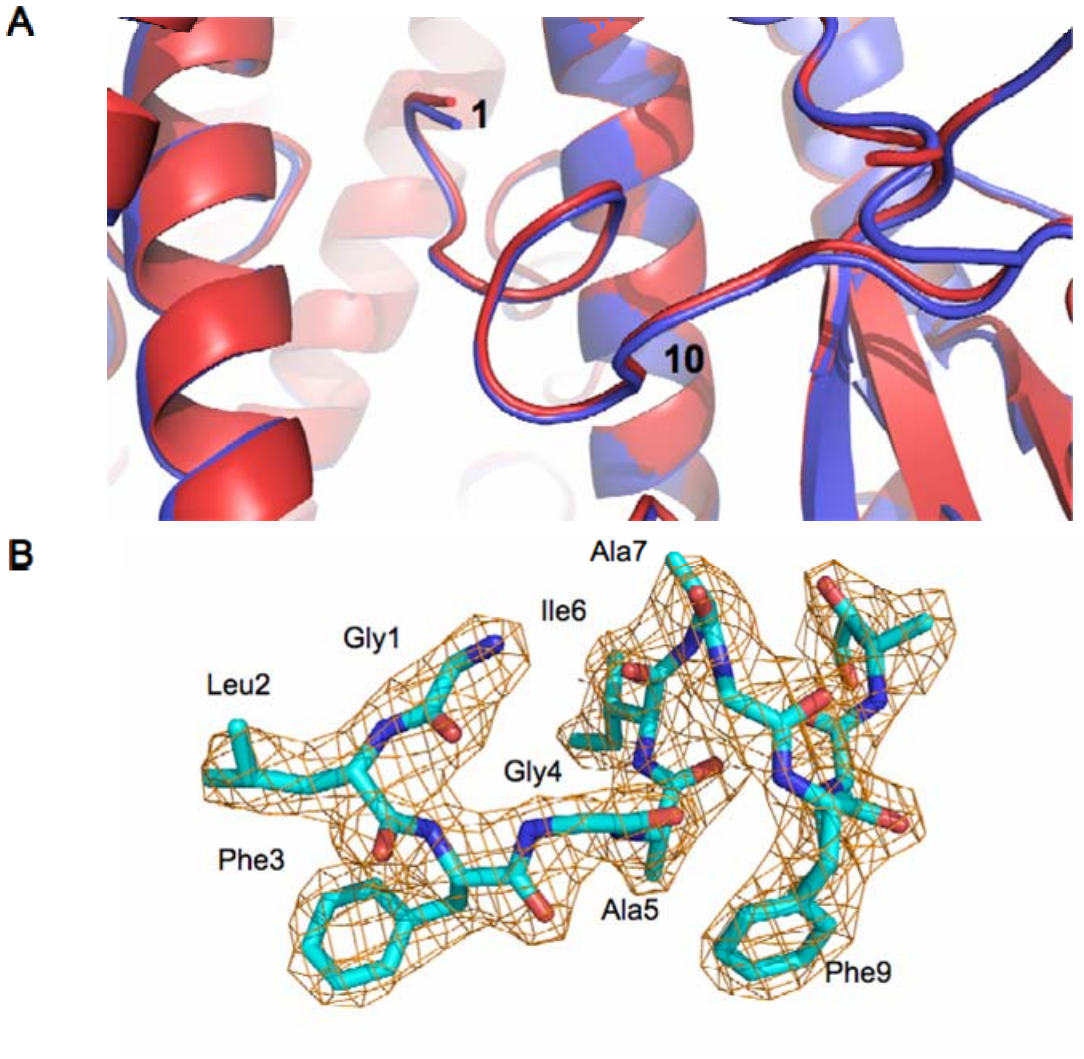

Fig. S3. **Electron density at the CR6261-SC1918/H1 interface.** The electron density maps are contoured at 2σ. The HCDRs 1 and 3 are depicted in yellow and the HA2 A-helix is shown in cyan.

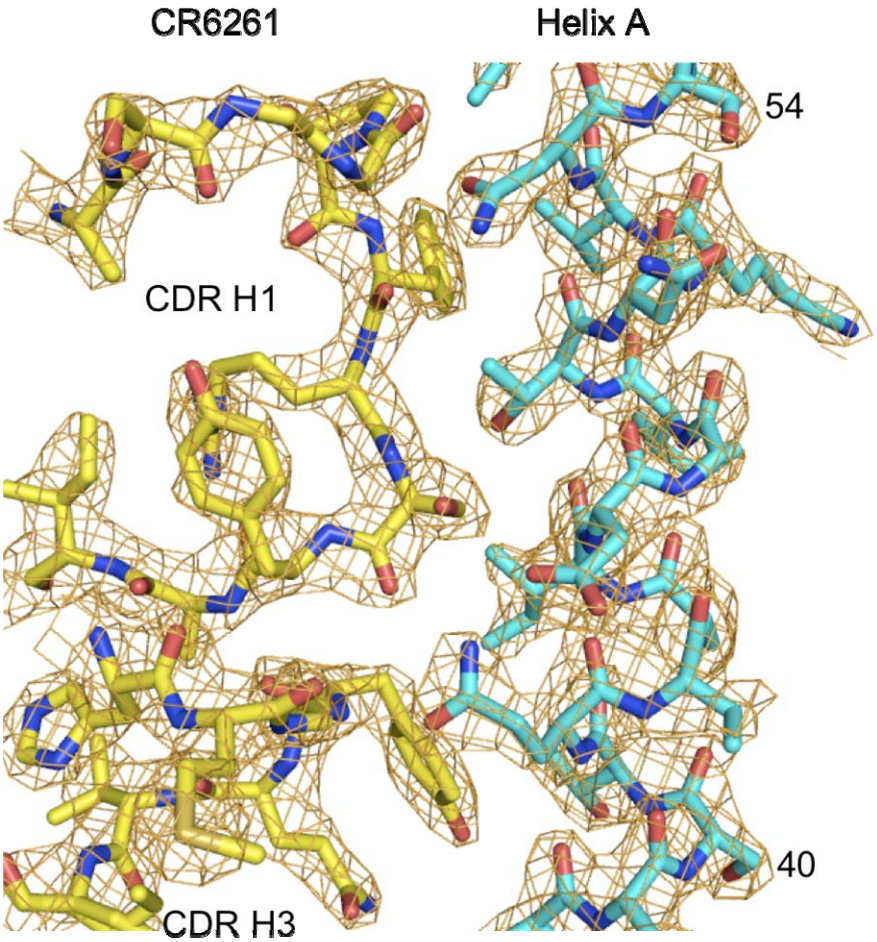

Fig. S4. **Conservation of the HA2 Asn154 glycosylation site across subtypes.** A consensus glycosylation site (Asn-Xaa-Ser/Thr) is present in 5241 of 5261 analyzed clones from all 16 subtypes. The values above each bar indicate the percent conservation for that subtype.

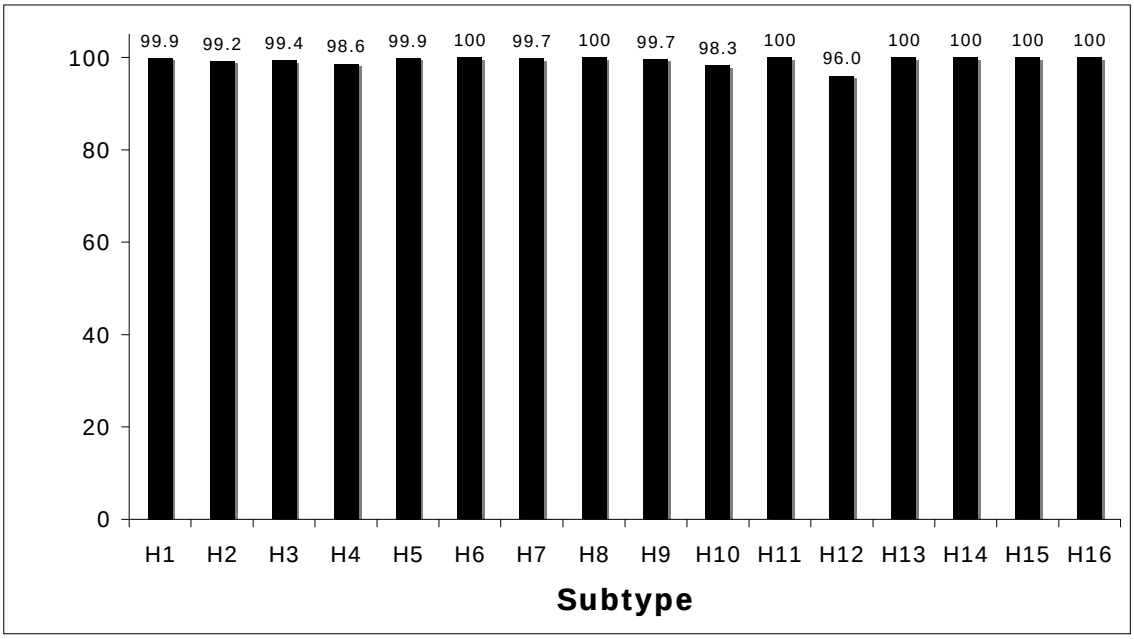

Fig. S5. **Interaction of CDR H2 (V_H 1-69) with a hydrophobic patch on the HA.** HCDR2 is colored in yellow with red residue labels corresponding to the hydrophobic tip. HA residues making hydrophobic contacts are colored blue with black labels.

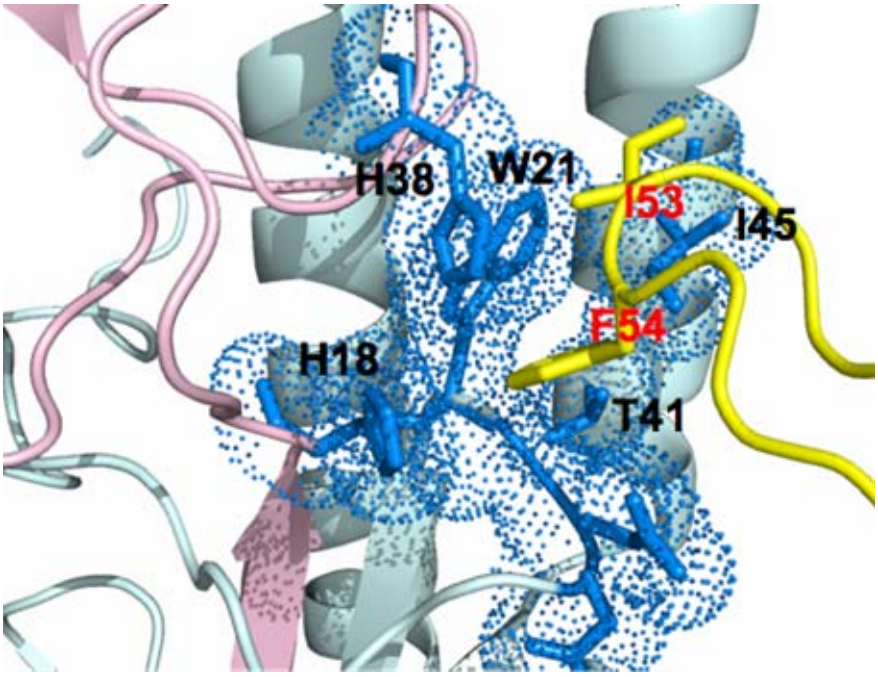

Fig. S6. **Conformational flexibility of the membrane distal end of SC1918 at acidic pH**. The SC1918/H1 HA (A) and Viet04/H5 HA (B) from the complex structures with CR6261 (not shown) are colored by B-value. The warmest colors (*i.e.*, red and orange) indicate highest B-values, while cool colors (*i.e.*, blue) indicate low B-values. The HA2 core and membrane proximal regions have low B-values and clear electron density in both structures, while the B-values at the top of HA1 are much higher and the electron density maps are less well-defined in the SC1918/H1 structure at low pH. In contrast, the B-values are lower and more uniform across the Viet04/H5 structure at higher pH, suggesting it is more rigid and less flexible.

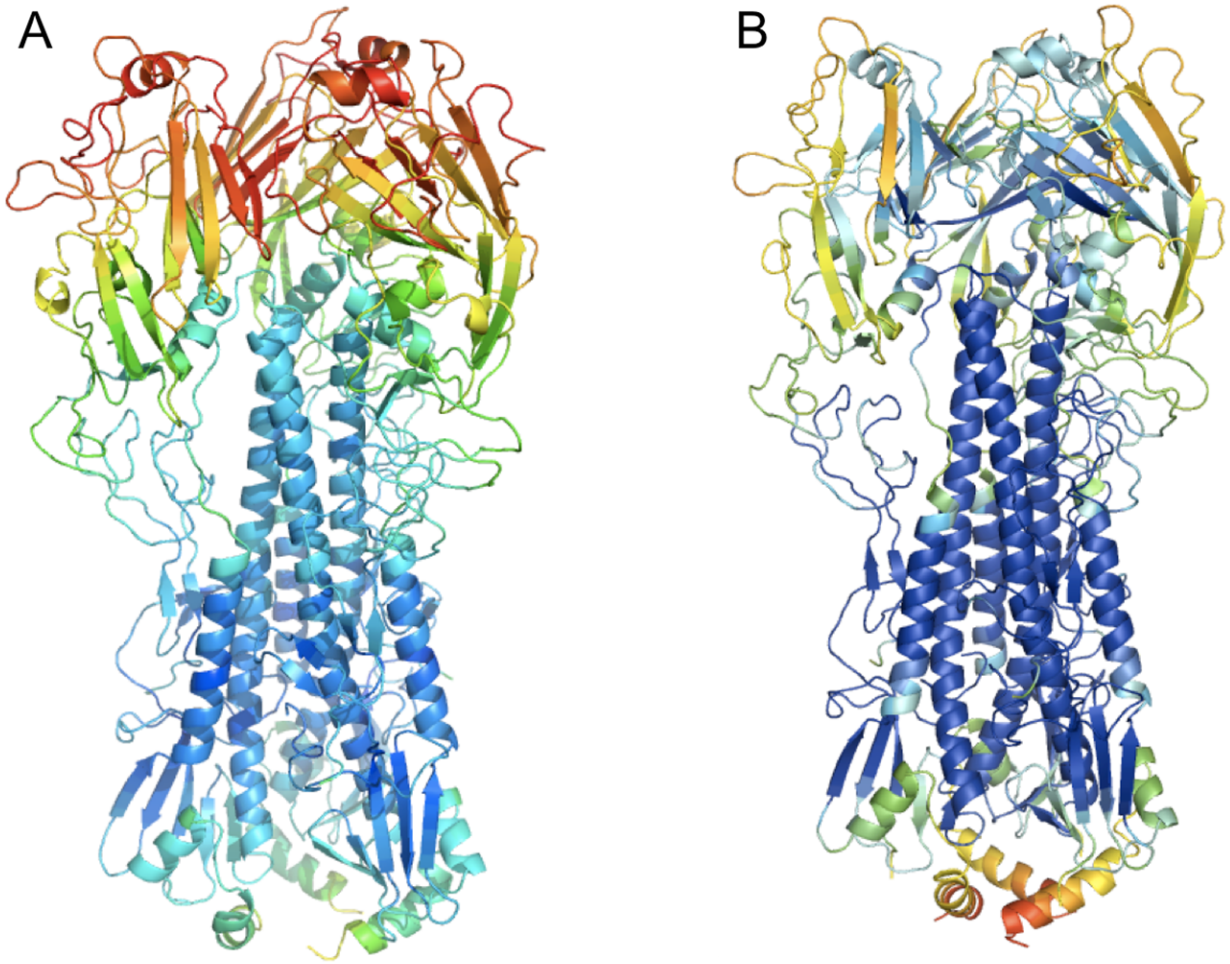

Fig. S7. **Conservation of the glycosylation site at Asn38 in HA1.** The glycosylation site at Asn38 in HA1 is highly conserved in the few subtypes that fail to bind CR6261 (H3, H7, H10—no data for H15) and is absent in all subtypes neutralized by CR6261. Values above bars indicated the percent of published sequences with an Asn-Xaa-Ser/Thr consensus motif at position 38.

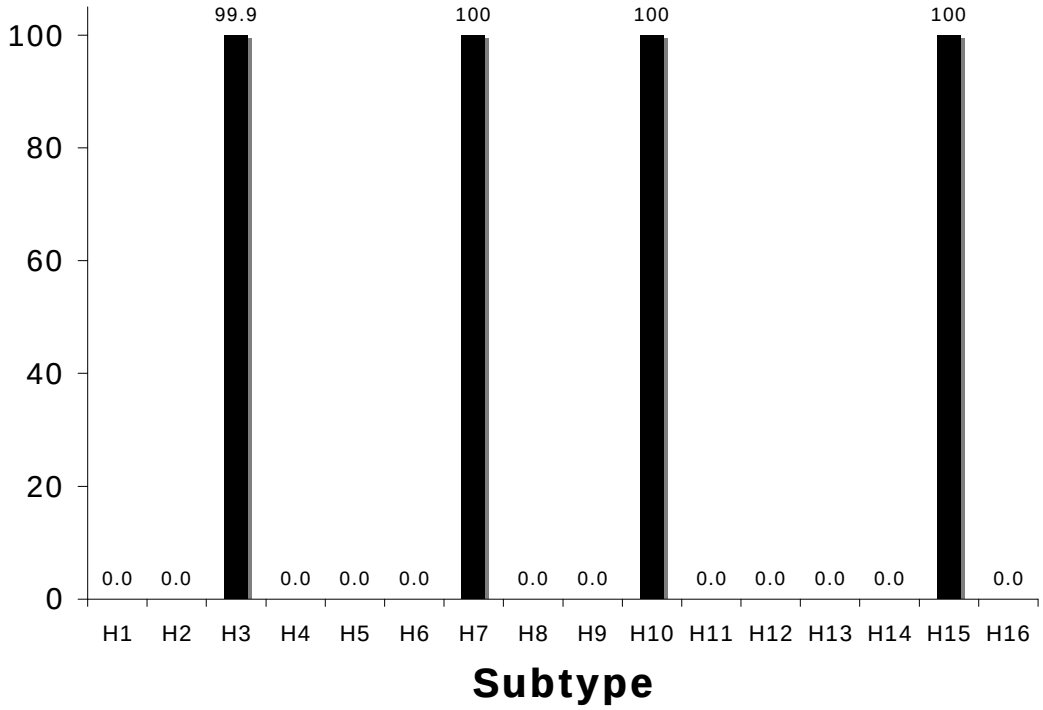

Table S1. Data collection and refinement statistics for the CRF6261-SC1918/H1 and CRF6261-Viet04/H5 complexes

Data collection	CRF6261-SC1918/H1	CRF6261-Viet04/H5
Beamline	APS GM/CA-CAT 23-IDB	APS GM/CA-CAT 23-IDB
Wavelength (Å)	1.03333	1.03333
Space group	$I2_13$	$P2_13$
Unit cell parameters	a = b = c = 202.39 Å	a = b = c = 202.76 Å
	$\alpha = \beta = \gamma = 90.00°$	$\alpha = \beta = \gamma = 90.00°$
Resolution (Å)	50 - 2.19 (2.24 – 2.19)[a]	49 - 2.70 (2.76 – 2.70) [a]
Observations	1,514,299	1,625,764
Unique reflections	71,438 (4,653) [a]	76,118 (7,761) [a]
Completeness (%)	100.0 (99.8) [a]	100.0 (99.9) [a]
$<I/\sigma_I>$	30.9 (2.32) [a]	18.4 (2.03) [a]
R_{sym}[b]	0.11 (0.79) [a]	0.13 (0.79) [a]
Refinement statistics		
Resolution	40 - 2.20 (2.26 – 2.20) [a]	40 - 2.70 (2.77 – 2.70) [a]
Reflections (total)	62,750	67,938
Reflections (test)	3,391	3,645
R_{cryst}(%)[c]	20.5	20.2
R_{free}(%)[d]	24.3	26.1
Average B-value (Å^2)	36.5	44.3[e]
Wilson B-value (Å^2)	56.6	81.4
Protein atoms	6,189	13,863
CHO atoms	78	148
Waters	293	164
Other	53	14
RMSD from ideal geometry		
Bond length (Å)	0.019	0.012
Bond angles (°)	1.78	1.43
Ramachandran statistics (%)[f]		
Favored	95.3	94.0
Outliers	0.9	0.8

[a] Numbers in parentheses refer to the highest resolution shell.

[b] $R_{sym} = \Sigma_{hkl} | <I_i-> | / \Sigma_{hkl} I_i$, where I_i is the scaled intensity of the i^{th} measurement and $< I_i >$ is the average intensity for that reflection.

[c] $R_{cryst} = \Sigma_{hkl} | F_o - F_c | / \Sigma_{hkl} | F_o |$ x 100

[d] R_{free} was calculated as for R_{cryst}, but on a test set comprising 5% of the data excluded from refinement.

[e] After TLS

[f] Calculated using Molprobity (S20).

Table S2. Hydrogen bonds between CR6261 and H1 and H5 HAs[a].

	CR6261-SC1918/H1		CR6261-Viet04/H5 [b]	
	Donor Residue	Acceptor Residue	Donor Residue	Acceptor Residue
1			HA1-Ser291OG	V_H-Asp72OD2
2	HA2-Gln42NE2	V_H-Ser31O	HA2-Gln42NE2	V_H-Ser31O
3	HA2-Thr49OG1	V_H-Arg30N		
4	HA2-Asn53ND2	V_H-Phe29O	HA2-Asn53ND2	V_H-Phe29O
5	V_H-Phe29N	HA2-Asn53OD1	V_H-Phe29N	HA2-Asn53OD1
6	V_H-Ser31OG	HA2-Asp46OD1	V_H-Ser31OG	HA2-Asp46OD1
7	V_H-Thr56OG1	HA2-Ile18O [c]		
8	V_H-Tyr98OH	HA2-Asp19O	V_H-Tyr98OH	HA2-Asp19O
9	V_H-Tyr98N	HA2-Gln42OE1	V_H-Tyr98N	HA2-Gln42OE1

[a] Hydrogen bonding interactions were calculated with HBPLUS (S16).
[b] For molecule 1 [HA chains A (HA1) & B (HA2), Fab chain E (V_H)] in the asymmetric unit of the crystal .
[c] Mediated by a bridging water molecule.

Table S3. Van der Waals' contacts between CR6261 and H1 and H5 HAs[a].

CR6261-SC1918/H1				CR6261-Viet04/H5			
HA Residue		V_H Residue	Contacts	HA Residue		V_H Residue	Contacts [b]
HA1	His18	Phe54	1				
HA1	His38	Ile53	4	HA1	His38	Ile53	1
HA1	His38	Phe54	3	HA1	His38	Phe54	4
HA1	Val40	Phe29	2	HA1	Gln40	Phe29	3
HA1	Val40	Phe74	3	HA1	Gln40	Phe74	5
HA1	Asn41	Phe74	2	HA1	Asp41	Phe74	2
HA1	Leu42	Phe74	2	HA1	Ile42	Phe74	2
				HA1	Ser291	Asp72	2
HA1	Ser291	Phe74	5	HA1	Ser291	Phe74	3
HA1	Ser291	Ala75	5				
HA1	Leu292	Phe74	6	HA1	Met292	Phe74	2
HA1	Pro293	Phe74	2	HA1	Pro293	Phe74	4
HA1	Thr318	Ile53	1	HA1	Thr318	Ile53	2
HA2	Asp19	Tyr98	3	HA2	Asp19	Tyr98	2
HA2	Asp19	Gln99	1				
HA2	Gly20	Phe54	6	HA2	Gly20	Phe54	2
HA2	Gly20	Tyr98	1	HA2	Gly20	Tyr98	1
HA2	Trp21	Ile53	2	HA2	Trp21	Ile53	2
HA2	Trp21	Phe54	5	HA2	Trp21	Phe54	6
HA2	Gln38	Tyr98	1	HA2	Lys38	Tyr98	1
HA2	Gln38	Gln99	3				
HA2	Thr41	Tyr98	7	HA2	Thr41	Tyr98	7
HA2	Gln42	Ser31	1	HA2	Gln42	Ser 31	1
HA2	Gln42	Gly97	3	HA2	Gln42	Gly97	3
HA2	Gln42	Tyr98	7	HA2	Gln42	Tyr98	6
HA2	Ile45	Ser31	2	HA2	Ile45	Ser31	3
				HA2	Ile45	Pro52A	1
HA2	Ile45	Phe54	1	HA2	Ile45	Phe54	1
HA2	Ile45	Tyr98	4	HA2	Ile45	Tyr98	4
HA2	Asp46	Ser31	2	HA2	Asp46	Ser31	2
HA2	Thr49	Phe29	1	HA2	Thr49	Phe29	3
HA2	Thr49	Arg30	2	HA2	Thr49	Arg30	5
HA2	Thr49	Ser31	1	HA2	Thr49	Ser31	1
HA2	Val52	Phe29	6	HA2	Val52	Phe29	6
HA2	Asn53	Gly27	7	HA2	Asn53	Gly27	7
HA2	Asn53	Pro28	1	HA2	Asn53	Pro28	2
HA2	Asn53	Phe29	7	HA2	Asn53	Phe29	4
HA2	Ile56	Pro28	2	HA2	Ile56	Pro28	1
HA2	Ile56	Phe29	2	HA2	Ile56	Phe29	2
HA2	Ile56	Phe74	2	HA2	Ile56	Phe74	1
		Total	116			Total	104

[a] Van der Waals' contacts were calculated using CONTACSYM (S17).
[b] Number of van der Waals' contacts in complex 1 (complex 2 has 122)

References

S1. I. A. Wilson, J. J. Skehel, D. C. Wiley, *Nature* **289**, 366 (1981).

S2. J. Stevens *et al.*, *Science* **312**, 404 (2006).

S3. J. Stevens *et al.*, *Science* **303**, 1866 (2004).

S4. E. Boel *et al.*, *J Immunol Methods* **239**, 153 (2000).

S5. Z. Otwinowski, W. Minor, *Methods Enzymol* **276**, 307 (1997).

S6. A. J. McCoy *et al.*, *J Appl Crystallogr* **40**, 658 (2007).

S7. S. J. Gamblin *et al.*, *Science* **303**, 1838 (2004).

S8. A. L. Corper *et al.*, *Nat Struct Biol* **4**, 374 (1997).

S9. G. N. Murshudov, A. A. Vagin, E. J. Dodson, *Acta Crystallogr D* **53**, 240 (1997).

S10. P. D. Adams *et al.*, *Acta Crystallogr D* **58**, 1948 (2002).

S11. P. Emsley, K. Cowtan, *Acta Crystallogr D* **60**, 2126 (2004).

S12. J. Painter, E. A. Merritt, *Acta Crystallogr D* **62**, 439 (2006).

S13. J. Painter, E. A. Merritt, *J Appl Crystallogr* **39**, 109 (2006).

S14. S. Yamada *et al.*, *Nature* **444**, 378 (2006).

S15. K. Cowtan, *Joint CCP4 and ESF-EACBM Newsletter on Protein Crystallography* **31**, 34 (1994).

S16. I. K. McDonald, J. M. Thornton, *J Mol Biol* **238**, 777 (1994).

S17. S. Sheriff, W. A. Hendrickson, J. L. Smith, *J Mol Biol* **197**, 273 (1987).

S18. M. Connolly, *J Appl Crystallogr* **16**, 548 (1983).

S19. S. Hayward, H. J. Berendsen, *Proteins* **30**, 144 (1998).

S20. J. S. Richardson, W. A. Bryan, 3rd, D. C. Richardson, *Methods Enzymol* **374**, 385 (2003).

S21. M. D. Abramoff, P. J. Magelhaes, S. J. Ram, *Biophotonics Internat* **11**, 36 (2004).